

TR-BREATH: Time-Reversal Breathing Rate Estimation and Detection

Chen Chen, *Student Member, IEEE*, Yi Han, Yan Chen, *Senior Member, IEEE*, Hung-Quoc Lai, Feng Zhang, *Student Member, IEEE*, Beibei Wang, *Senior Member, IEEE*, and K. J. Ray Liu, *Fellow, IEEE*

Abstract—In this paper, we introduce TR-BREATH, a time-reversal (TR) based contact-free breathing monitoring system. It is capable of breathing detection and multi-person breathing rate estimation within a short period of time using off-the-shelf WiFi devices. The proposed system exploits the channel state information (CSI) to capture the miniature variations in the environment caused by breathing. To magnify the CSI variations, TR-BREATH projects CSIs into the TR resonating strength (TRRS) feature space and analyzes the TRRS by the Root-MUSIC and affinity propagation algorithms. Extensive experiment results indoor demonstrate a perfect detection rate of breathing. With only 10 seconds of measurement, a mean accuracy of 99% can be obtained for single-person breathing rate estimation under the non-line-of-sight (NLOS) scenario. Furthermore, it achieves a mean accuracy of 98.65% in breathing rate estimation for a dozen people under the line-of-sight (LOS) scenario and a mean accuracy of 98.07% in breathing rate estimation of 9 people under the NLOS scenario, both with 63 seconds of measurement. Moreover, TR-BREATH can estimate the number of people with an error around 1. We also demonstrate that TR-BREATH is robust against packet loss and motions. With the prevailing of WiFi, TR-BREATH can be applied for in-home and real-time breathing monitoring.

Index Terms—Channel state information, time-reversal, breathing rate estimation, breathing detection.

I. INTRODUCTION

Breathing rate is an important vital indicator for the health status and predictor of medical conditions [1]. Breathing monitoring is the key technology in the future medical care system. Nevertheless, most conventional breathing monitoring methods are invasive in that they require physical contact with human bodies.

Contact-free breathing monitoring schemes are developed to overcome the drawbacks of conventional schemes for in-home breathing monitoring. Among them, schemes driven by radio frequency (RF) techniques are the most promising candidates due to their abilities to sense breathing in a highly complicated indoor environment by leveraging the propagation of electromagnetic (EM) waves. In terms of techniques, these schemes can be classified into radar-based and WiFi-based. Among the radar-based schemes, Doppler radar is commonly

used which measures the frequency shift of the signals caused by the periodic variations of the EM waves reflected from human bodies [2]. Recently, Adib *et al.* present a vital sign monitoring system that uses the Universal Software Radio Peripheral (USRP) as the RF front-end to emulate a frequency modulated continuous radar (FMCW) [3]. However, the requirement of specialized hardware hinders the deployment of these schemes.

On the other hand, WiFi-based schemes are infrastructure-free since they are built upon the existing WiFi networks available indoor. Received signal strength indicator (RSSI) is often used due to its availability on most WiFi devices. In [4], Abdelnasser *et al.* present UbiBreathe that harnesses RSSI on WiFi devices for breathing estimation. However, UbiBreathe is accurate only when users hold the WiFi devices close to their chests. Another exploitable information on WiFi devices is the channel state information (CSI), a fine-grained information that portrays the EM wave propagation. The scheme proposed by Liu *et al.* in [5] is one of the first few CSI-based breathing monitoring approaches. Nevertheless, they assume the number of people to be known. Moreover, periodogram is used for spectral analysis that needs a relatively long time for accurate breathing monitoring. In [6], Chen *et al.* demonstrate the feasibility of high accuracy multi-person breathing rate estimation using CSIs by leveraging the Root-MUSIC algorithm [7].

In this work, we propose TR-BREATH, a WiFi-based contact-free breathing monitoring system leveraging time-reversal (TR) technique that detects and monitors multi-person breathing. TR technique is a promising paradigm for future internet-of-things applications [8]. The TR technique is utilized for centimeter-level indoor localization [9]–[12], speed estimation [13], human biometrics [14], and event detection [15]. In this paper, we demonstrate that TR could also capture the minor but periodic variations embedded in the CSIs.

TR-BREATH measures the CSI variations via the time-reversal resonating strength (TRRS) [16]. The TRRS values are further analyzed by the Root-MUSIC algorithm to produce breathing rate candidates. Then, key statistics are derived based on these candidates to facilitate breathing detection. If breathing is detected, TR-BREATH estimates the multi-person breathing rates via affinity propagation [17], likelihood assignment, and cluster merging. Based on the cluster likelihoods, TR-BREATH could formulate an estimation on the number of people. Also, TR-BREATH makes full use of the sequence numbers in WiFi packets to enhance its robustness against

Chen Chen, Yi Han, Hung-Quoc Lai, Feng Zhang, Beibei Wang, and K. J. Ray Liu are with Origin Wireless Inc., Greenbelt, MD 20770, United States. Chen Chen, Feng Zhang, Beibei Wang, and K. J. Ray Liu are also with the Department of Electrical and Engineering, University of Maryland College Park, College Park, MD 20742 United States (e-mail: {cc8834, fzhang15, bebewang, kjrlui}@umd.edu). Yan Chen was with Origin Wireless Inc., and now with University of Electronic Science and Technology of China, Chengdu, Sichuan, China (e-mail: eecyan@uestc.edu.cn). Yi Han and Hung-Quoc Lai are with Origin Wireless Inc. (e-mail: {yi.han, quoc.lai}@originwireless.net).

packet loss which is common in areas with densely deployed WiFi devices.

Extensive experiments in an office environment show that TR-BREATH achieves perfect detection on the existence of breathing within 63 seconds of measurements. Moreover, with only 10 seconds of measurements, TR-BREATH achieves 99% accuracy for single-person breathing rate estimation under NLOS. For multi-person breathing monitoring, TR-BREATH achieves a mean accuracy of 98.65% for a dozen people under LOS and 98.07% for 9 people under NLOS, both with 63 seconds of measurement. With the knowledge of the maximum number of people, TR-BREATH can count the people number with an error around 1.

TR-BREATH differs from the prior works in the following ways:

- It is infrastructure-free since it utilizes off-the-shelf WiFi devices, while the schemes in [2], [3], [18] require dedicated hardware.
- With the Root-MUSIC algorithm, TR-BREATH can achieve highly accurate breathing rate estimations within 10 seconds, much shorter than the periodogram schemes used in [3] and [5] so that real-time breathing monitoring is viable.
- It can resolve the breathing rates of 9 people breathing concurrently, while in [3] and [5], the authors merely show the results for up to 3 people.
- It integrates both breathing detection and estimation, while [3], [5], [6] only emphasize breathing rate estimation.
- It can estimate the number of people, which is assumed to be known in advance in [3], [5], [6].
- It is robust against packet loss in the presence of ambient WiFi traffic, while [3], [5], [6] ignore this practical issue.

The rest of the paper is organized as follows. Section II presents an intuitive CSI model that encapsulates the effect of breathing, ambient WiFi traffic, and motions, followed by a brief introduction to the Root-MUSIC algorithm that extracts breathing rates. Section III elaborates on the algorithm of TR-BREATH. Section IV demonstrates the experiment results for both single-person and multi-person LOS and NLOS scenarios. Section V demonstrates the performances of TR-BREATH in the presence of a few practical issues. Future research directions are discussed in Section VI. Finally, Section VII concludes the paper.

II. THEORETICAL FOUNDATION

In this section, we first present the CSI model in a static environment without dynamics. Then, we extend the model by considering environmental dynamics, motions, and ambient WiFi traffic. After that, we introduce TRRS as a feature that captures the CSI variations. Finally, we introduce the Root-MUSIC algorithm for breathing rate estimations.

A. CSI Model without Environmental Dynamics

In the absence of dynamics, the CSI on subcarrier k at time t denoted by $H_k(t)$ can be written as

$$H_k(t) = \sum_{\ell=1}^L \zeta_{\ell} e^{-j2\pi \frac{d_{\ell}}{\lambda_k}} + e_k(t), \quad (1)$$

where $k \in \mathcal{V}$ and \mathcal{V} denotes the set of usable subcarriers with a cardinality of V , i.e., V usable subcarriers, L is the total number of multipath components (MPC), ζ_{ℓ} is the complex gain of MPC ℓ , d_{ℓ} is the length of MPC ℓ , and λ_k is the wavelength of subcarrier k given by

$$\lambda_k = \frac{c}{f_c + \frac{k}{N_{\text{DFT}} T_s}}, \quad (2)$$

where f_c is the carrier frequency, c is the speed of the light, T_s is the sampling interval given as $T_s = \frac{1}{B}$ where B is the baseband bandwidth of the WiFi signals, and N_{DFT} is the size of discrete Fourier Transform (DFT). $e_k(t)$ is the thermal noise on subcarrier k at time t . The MPC gains and delays are time-invariant.

B. CSI Model with Breathing Impact

With breathing, one or more MPC gains and delays become time-varying. For simplicity, we assume that breathing only affects MPC #1. Then, the gain of MPC #1 takes the form [19]

$$\zeta_1(t) = \zeta_1 \times \left(1 + \frac{\Delta d_1}{d_1} \sin \theta \sin \left(\frac{2\pi b}{60} t + \phi \right) \right)^{-\psi} \quad (3)$$

where ζ_1 and d_1 are the gain and length for MPC #1 without breathing, Δd_1 is the additional positional displacement of MPC #1 caused by breathing, ψ is the path-loss exponent, θ is the angle between the subject and the impinging EM wave, b is the breathing rate measured in breath-per-minute (BPM), ϕ is the initial phase of breathing. Given that $d_1 \gg \Delta d_1$, we can approximate $\zeta_1(t)$ with the time-invariant MPC gain ζ_1 .

On the other hand, breathing affects the phase of MPC #1 by changing its path length $d_1(t)$ expressed as

$$d_1(t) = d_1 + \Delta d_1 \sin \theta \sin \left(\frac{2\pi b}{60} t + \phi \right). \quad (4)$$

Now, $H_k(t)$ takes the form

$$H_k(t) = \zeta_1 e^{-j2\pi \frac{d_1(t)}{\lambda_k}} + \sum_{\ell=2}^L \zeta_{\ell} e^{-j2\pi \frac{d_{\ell}}{\lambda_k}} + e_k(t), \quad (5)$$

which can be further written as

$$H_k(t) = \zeta_1 e^{-j2\pi \frac{d_1}{\lambda_k}} e^{-j2\pi \frac{\Delta d_1 \sin \theta \sin \left(\frac{2\pi b}{60} t + \phi \right)}{\lambda_k}} + \sum_{\ell=2}^L \zeta_{\ell} e^{-j2\pi \frac{d_{\ell}}{\lambda_k}} + e_k(t). \quad (6)$$

The first term on the right hand side of $H_k(t)$ in (6) can be decomposed into an infinite summation according to the Jacobi-Anger expansion [20], as

$$e^{-j2\pi \frac{\Delta d_1 \sin \theta \sin(\frac{2\pi b}{60} t + \phi)}{\lambda_k}} = \sum_{m=-\infty}^{+\infty} (-1)^m J_m(\nu_k) e^{jm \frac{2\pi b}{60} t} e^{jm\phi} \quad (7)$$

where $\nu_k = 2\pi \sin \theta \Delta d_1 / \lambda_k$ and $J_m(x)$ is the m -th order Bessel function with argument x . It can be seen that in addition to the spectral line at b , there also exists an infinite number of harmonics with spectral lines at mb where m is a non-zero integer.

In practice, $J_m(\nu_k)$ decays quickly for $|m| \geq 2$ given the typical values of ν_k . Thus, (7) can be approximated as

$$e^{-j2\pi \frac{\Delta d_1 \sin \theta \sin(\frac{2\pi b}{60} t + \phi)}{\lambda_k}} \approx \sum_{m=-1}^{+1} (-1)^m J_m(\nu_k) e^{jm \frac{2\pi b}{60} t} e^{jm\phi} \quad (8)$$

which consists of two spectral lines at $\pm b$ with respect to $m = \pm 1$ as well as a DC component with respect to $m = 0$. Thus, $H_k(t)$ can be expressed as

$$H_k(t) \approx \underbrace{\zeta_1 e^{-j2\pi \frac{d_1}{\lambda_k}} \sum_{m=-1}^{+1} (-1)^m J_m(\nu_k) e^{jm \frac{2\pi b}{60} t} e^{jm\phi}}_{S_k(t)} + \underbrace{\sum_{\ell=2}^L \zeta_\ell e^{-j2\pi \frac{d_\ell}{\lambda_k}}}_{I_k} + e_k(t), \quad (9)$$

where $S_k(t)$ stands for the useful signal for breathing monitoring on subcarrier k , and I_k represents the time-invariant part due to the static environment and regarded as the interference. Notice that the dynamic model of $H_k(t)$ shown in (9) can be extended easily to the multi-person case.

C. Impact of Non-idealities on CSIs

In practice, we need to consider two random non-idealities in the CSI model:

- **Random phase distortion** caused by the differences between the local oscillators of the WiFi transmitter and receiver, which consists of an initial and a linear phase distortion.
- **Random amplitude variation** due to the automatic gain control (AGC) in the RF front-end that scales the input voltage into the dynamic range of the analog-to-digital converter (ADC).

With these two non-idealities, $H_k(t)$ in (9) should be modified as

$$H_k(t) = \Gamma(t) (S_k(t) + I_k) e^{j(\omega(t) + \kappa(t)k)} + e_k(t), \quad (10)$$

where $\Gamma(t)$ is the real-valued AGC gain at time t , $\omega(t)$ is the initial phase distortion at time t , and $\kappa(t)$ is the linear phase distortion at time t .

D. Impact of Motions on CSIs

The propagation of EM wave is affected by the motions of the subject under breathing monitoring such as turning heads or bending forward, known as the subject motion, as well as by

the motion caused by nearby people and/or objects not under monitoring, known as the ambient motion. Next, we present the CSI model incorporating both effects.

1) *Subject Motion*: When there exists subject motion, we need to partition time t into two time durations: the time duration without subject motion denoted as \mathcal{T}_{sm} , and the time duration with subject motion denoted as \mathcal{T}_{sm}^c , which is the complementary of \mathcal{T}_{sm} . Then, $S_k(t)$ is modified as

$$S_k(t) = \begin{cases} S_k^0(t) & , t \in \mathcal{T}_{sm} \\ S_k'(t) & , t \in \mathcal{T}_{sm}^c \end{cases}, \quad (11)$$

where $S_k^0(t)$ is the original breathing signal and $S_k'(t)$ is a random signal caused by the subject motion.

2) *Ambient Motion*: In the presence of ambient motion, I_k in (10) becomes time-variant and thus (10) should be rewritten as

$$H_k(t) = \Gamma(t) (S_k(t) + I_k(t)) e^{j(\omega(t) + \kappa(t)k)} + e_k(t). \quad (12)$$

The ambient motion $I_k(t)$ can be either periodic or non-periodic. For instance, $I_k(t)$ can be caused by the breathing of another person in the vicinity of the person under monitoring, or produced by the random motion of nearby people and objects. Clearly, $I_k(t)$ incurs interference into breathing monitoring. In this paper, we consider the ambient motion as bursty by affecting a portion of the monitoring duration, i.e.,

$$I_k(t) = \begin{cases} I_k^0(t) & , t \in \mathcal{T}_{am} \\ 0 & , t \in \mathcal{T}_{am}^c \end{cases}, \quad (13)$$

where \mathcal{T}_{am} is the continuous time duration with ambient motion while \mathcal{T}_{am}^c is the duration without ambient motion, and $I_k^0(t)$ is the original ambient motion signal.

E. Impact of Ambient WiFi Traffic on CSIs

In reality, CSIs are sampled with a time interval of T_{sp} with an initial time given as t_0 . The i -th CSI, denoted by $H_k[i]$, is sampled at the i -th time instant with a sequence number of $s_i = s_0 + i$. Its reception time is given by $t_i = t_0 + iT_{sp}$, where s_0 is the sequence number of the first CSI sample. Yet, due to the ambient WiFi traffic on the same WiFi channel, packet loss is unavoidable, leading to a sequence number $s_i \neq s_0 + i$ and a reception time $t_i = t_0 + (s_i - s_0)T_{sp} \neq t_0 + iT_{sp}$.

F. Overall CSI Model

Considering all effects discussed in Section II-C, Section II-D, and Section II-E, the discrete CSI model takes the form of

$$H_k[i] = \Gamma[i] (S_k[i] + I_k[i]) e^{j(\omega[i] + \kappa[i]k)} + e_k[i], \quad (14)$$

where $S_k[i]$ and $I_k[i]$ are the discrete signal and interference of the i -th CSI as defined in (11) and (13), $\Gamma[i]$ and $e_k[i]$ are the discrete AGC gain and thermal noise, and $S_k[i]$ and $I_k[i]$ are given as

$$S_k[i] = \begin{cases} S_k^0[i] & , i \in \mathbb{T}_{sm} \\ S_k'[i] & , i \in \mathbb{T}_{sm}^c \end{cases}, \quad (15)$$

$$I_k[i] = \begin{cases} I_k^0[i] & , i \in \mathbb{T}_{am} \\ 0 & , i \in \mathbb{T}_{am}^c \end{cases}, \quad (16)$$

where \mathbb{T}_{sm} and \mathbb{T}_{am} are the discrete CSI time index affected by subject motion and ambient motion respectively, while \mathbb{T}_{sm}^c and \mathbb{T}_{am}^c are the complementary discrete time index sets with respect to \mathbb{T}_{sm} and \mathbb{T}_{am} .

G. Calculating TRRS from CSIs

TRRS is used as a measure of similarity between any two CSIs. Different from the calculation of TRRS in the time domain as shown in [12], we calculate the TRRS between the i -th received CSI and the j -th received CSI in the frequency domain based on $H_k[i]$ and $H_k[j]$ in (14) as follows:

$$\text{TR}[\mathbf{H}[i], \mathbf{H}[j]] = \frac{\sum_{k \in \mathcal{V}} H_k[i] H_k^*[j] e^{-j(\omega^* + \kappa^* k)}}{\|\mathbf{H}[i]\|_2 \|\mathbf{H}[j]\|_2}, \quad (17)$$

where $\mathbf{H}[i] = \{H_k[i]\}_{k \in \mathcal{V}}$ and $\|\mathbf{x}\|_2$ is the ℓ_2 norm of the vector \mathbf{x} . ω^* and κ^* in (17) are introduced to remove the initial and linear phase distortions, which are given by

$$\kappa^* = \arg \max_{\kappa} \left| \sum_{k \in \mathcal{V}} H_k[i] H_k^*[j] e^{-j\kappa k} \right| \quad (18)$$

$$\omega^* = \angle \left(\sum_{k \in \mathcal{V}} H_k[i] H_k^*[j] e^{-j\kappa^* k} \right)^* \quad (19)$$

The denominator of (17) normalizes the TRRS so that $\text{TR}[\mathbf{H}[i], \mathbf{H}[j]] \in [0, 1]$. In other words, the denominator mitigates the impact of the random gains $\Gamma[i]$ and $\Gamma[j]$. $\angle(x)$ is the operator that extracts the phase from the complex argument x .

H. Extracting Breathing Rates using Root-MUSIC

Root-MUSIC is a variant to the well-known Multiple Signal Classification (MUSIC) algorithm [21]. It is a super-resolution subspace-based spectral analysis algorithm widely used in signal processing applications [7]. Assume a total of N CSIs sampled uniformly with an interval of T_{sp} , we can calculate the $N \times N$ TRRS matrix \mathbf{R} based on (17), with the (i, j) -th element of \mathbf{R} given as $\text{TR}[\mathbf{H}[i], \mathbf{H}[j]]$.

After calculating \mathbf{R} , we perform an eigenvalue decomposition (EVD) on \mathbf{R} to produce

$$\mathbf{R} = \mathbf{U} \mathbf{\Lambda} \mathbf{U}^\dagger, \quad (20)$$

where \dagger is the transpose and conjugate operator, \mathbf{U} is a $N \times N$ orthonormal matrix such that $\mathbf{U}^\dagger \mathbf{U} = \mathbf{I}$ where \mathbf{I} is a $N \times N$ identity matrix, and $\mathbf{\Lambda}$ is a $N \times N$ diagonal matrix with descending real-valued diagonal entries equivalent to the eigenvalues of \mathbf{R} .

Secondly, the orthonormal matrix \mathbf{U} is decomposed into a signal subspace and a noise subspace. The signal subspace, denoted by \mathbf{U}_s , consists of the first p columns of \mathbf{U} , where $p \leq N - 1$ is the signal subspace dimension. On the other hand, the noise subspace, denoted by \mathbf{U}_n , consists of the last $N - p$ columns of \mathbf{U} .

Next, we calculate the matrix $\mathbf{Q} = \mathbf{U}_n \mathbf{U}_n^\dagger$. Then, we formulate the polynomial $f(z)$ as

$$f(z) = \sum_{m=0}^{N-1} \sum_{n=0}^{N-1} [\mathbf{Q}]_{m,n} z^{g_{m,n}}, \quad (21)$$

where $[\mathbf{Q}]_{m,n}$ is the (m, n) -th element of \mathbf{Q} , $z = e^{-j \frac{2\pi b T_{sp}}{60}}$, and $g_{m,n}$ is the *discrete difference function* highlighting the time difference between two CSI samples normalized to T_{sp} , given as

$$g_{m,n} = \begin{cases} s_m - s_n, & \text{Considering Packet Loss} \\ m - n, & \text{Otherwise.} \end{cases} \quad (22)$$

Notice that, by using $g_{m,n} = s_m - s_n$, the Root-MUSIC algorithm is robust against WiFi packet loss. Yet, when the ambient WiFi traffic is not severe, setting $g_{m,n}$ as $m - n$ suffices to produce accurate results.

Solving $f(z) = 0$ in (21) results in $2N - 2$ complex roots denoted by $\hat{\mathbf{z}} = \{\hat{z}_1, \hat{z}_2, \hat{z}_3, \dots, \hat{z}_{2N-2}\}$. Since \mathbf{Q} is Hermitian, if \hat{z} is a complex root of $f(z) = 0$, then $1/\hat{z}^*$ is also a complex root of $f(z) = 0$. In other words, the roots of $f(z) = 0$ come in pairs. Considering that only the phase of the complex roots carry the information about the breathing rates, we keep the $N - 1$ complex roots inside the unit circle. Then, we choose p out of the $N - 1$ complex roots closest to the unit circle. The breathing rate estimation can be formulated as

$$\hat{b}_i = 60 \times \frac{\angle \hat{z}_i}{2\pi T_{sp}}, \quad i = 1, 2, \dots, p. \quad (23)$$

From (12), we find that, while some complex roots are associated with breathing rates, the rest of these complex roots are produced by the motion interference and thermal noise. In particular, the power of the motion interference $I_k(t)$ can be even stronger than the breathing signal $S_k(t)$, e.g., when the motion happens very close to the WiFi devices capturing CSIs. As shown in Section V, as long as the WiFi devices are far away from the motions, the impact of motion can be largely neglected, and most of the complex roots of $f(z)$ in (21) are still associated with breathing.

Moreover, we realize that the breathing rates are limited to a finite range $[b_{\min}, b_{\max}]$ since people cannot breathe either too fast or too slow. Thus, we sift the breathing rate estimations $\hat{\mathbf{b}} = [\hat{b}_1, \hat{b}_2, \dots, \hat{b}_p]$ by discarding those outside the range of $[b_{\min}, b_{\max}]$, which leads to $\tilde{\mathbf{b}} = [\hat{b}_{r_1}, \hat{b}_{r_2}, \dots, \hat{b}_{r_{p'}}]$, where p' is the number of the remaining complex roots and r_i is the index of the i -th remaining estimation.

III. ALGORITHM

The architecture of TR-BREATH is illustrated in Fig. 1. We assume the availability of CSIs on a total of D links in a multi-antenna WiFi system. In the following parts, we elaborate on the details of the algorithms in TR-BREATH.

A. CSI Calibration

The miniature and periodic changes in CSIs are masked by the phase distortions caused by residual synchronization errors. To overcome this issue, in the calculation of TRRS, we evaluate κ^* and ω^* according to (18) and (19). This step is executed on all links in parallel.

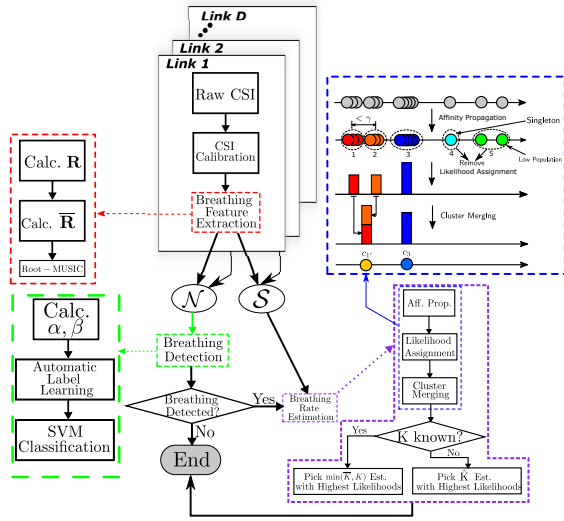


Fig. 1: Overview of the architecture of TR-BREATH

B. Breathing Feature Extraction

1) *Calculating the TRRS Matrix:* Assume that we obtain N CSIs for each link. Since breathing is not strictly stationary in the long run, calculating the $N \times N$ TRRS matrix \mathbf{R} using the calibrated CSIs according to (17) is not optimal which degrades the performance. So, TR-BREATH divides the duration of measurements into multiple blocks, where each block consists of M CSIs where $M \leq N$. Assume that two blocks overlap by P CSIs, TR-BREATH can obtain a total of $B = \lfloor \frac{N-P}{M} \rfloor + 1$ blocks.

For each block, TR-BREATH further partitions the block duration into several overlapping time windows with W CSIs for each, with the CSIs associated with the i -th time window given by $\{\mathbf{H}[i], \mathbf{H}[i+1], \dots, \mathbf{H}[i+W-1]\}$. Two adjacent time windows overlap by 1 CSI.

2) *Temporal Smoothing of the TRRS Matrix:* To suppress the spurious estimations due to interference and noise, TR-BREATH performs temporal smoothing on the TRRS matrix for each block taking the packet loss into consideration. Firstly, for link d , block b , TR-BREATH parses the sequence numbers for the M CSIs inside that block, denoted as $s_{b(N-P)+1}, s_{b(N-P)+2}, \dots, s_{b(N-P)+M}$. Then, TR-BREATH calculates the difference M' between the maximum sequence number $s_{\max} = s_{b(N-P)+M}$ and the minimum sequence number $s_{\min} = s_{b(N-P)+1}$. If $M' = s_{\max} - s_{\min} > M$, we infer that $M' - M$ WiFi packets are missing due to ambient WiFi traffic.

Secondly, TR-BREATH calculates the $M \times M$ TRRS matrix for link d and block b according to (17), denoted as $\mathbf{R}_{b,d}$. Then, TR-BREATH forms an extended TRRS matrix $\mathbf{R}'_{b,d}$ with dimension $M' \times M'$. The entries of $\mathbf{R}'_{b,d}$ are initialized with zeros. Then, TR-BREATH fills the (s_i, s_j) -th entry of $\mathbf{R}'_{b,d}$ with the (i, j) -th element of $\mathbf{R}_{b,d}$. Equivalently speaking, $\mathbf{R}'_{b,d}$ is an interpolated version of $\mathbf{R}_{b,d}$, with entries of zero

standing for the index of the missing packets¹. With a time window size W , TR-BREATH could formulate $Z = M' - W + 1$ time windows in total. Meanwhile, TR-BREATH forms a counting matrix $\mathbf{C}'_{b,d}$ for link d and block b such that

$$[\mathbf{C}'_{b,d}]_{i,j} = \begin{cases} 1, & \text{If } [\mathbf{R}'_{b,d}]_{i,j} > 0 \\ 0, & \text{Otherwise.} \end{cases} \quad (24)$$

Next, TR-BREATH partitions $\mathbf{R}'_{b,d}$ into Z square submatrix, with the z -th submatrix given by $\mathbf{R}'_{b,d,z}$ composed by the entries of $\mathbf{R}_{b,d}$ from row z to row $z+W-1$ and column z to column $z+W-1$. The same operation is performed on $\mathbf{C}'_{b,d}$, leading to Z square submatrix $\{\mathbf{C}'_{b,d,z}\}_{z=1,2,\dots,Z}$. $\{\mathbf{R}'_{b,d,z}\}_{z=1,2,\dots,Z}$ and $\{\mathbf{C}'_{b,d,z}\}_{z=1,2,\dots,Z}$ are accumulated as $\overline{\mathbf{R}}'_{b,d} = \sum_{z=1}^Z \mathbf{R}'_{b,d,z}$ and $\overline{\mathbf{C}}'_{b,d} = \sum_{z=1}^Z \mathbf{C}'_{b,d,z}$. Also, we replace the sequence numbers with $[1, 2, \dots, W]$.

Then, we locate and delete the rows and columns of $\overline{\mathbf{R}}'_{b,d}$ and $\overline{\mathbf{C}}'_{b,d}$ with at least one zero, resulting in the matrix $\overline{\mathbf{R}}''_{b,d}$ and $\overline{\mathbf{C}}''_{b,d}$, both with dimension $W' \times W'$ where $W' \leq W$. The deleted index are also removed from the updated sequence numbers in the previous step, leading to the updated sequence numbers $s''_1, s''_2, \dots, s''_{W'}$.

Finally, we calculate the temporal smoothed matrix $\overline{\mathbf{R}}_{b,d}$ with its (i, j) -th element given by $[\overline{\mathbf{R}}''_{b,d}]_{i,j} / [\overline{\mathbf{C}}''_{b,d}]_{i,j}$ for further processing. Fig. 2 shows an example of generating $\overline{\mathbf{R}}_{b,d}$ under $N = 5, M = 4, M' = 5, W = 4, W' = 2, P = 1$, and $B = 2$. Notice that the parameters indicate the lost of one WiFi packet since $M' - M = 1$.

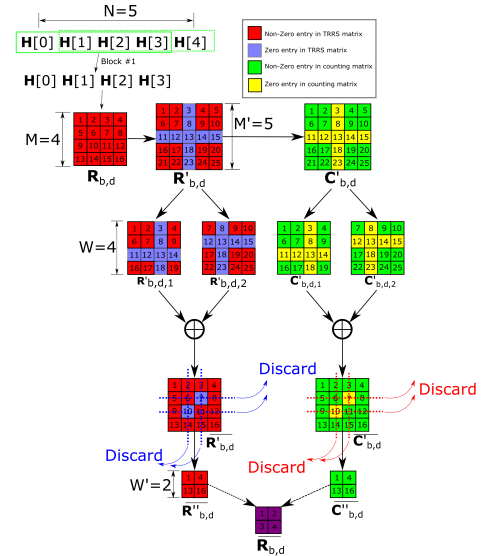


Fig. 2: Procedure of TRRS matrix smoothing

3) *Analysis via Root-MUSIC:* The smoothed $W' \times W'$ TRRS matrix $\overline{\mathbf{R}}_{b,d}$ is analyzed via the Root-MUSIC algorithm. An EVD is invoked on $\overline{\mathbf{R}}_{b,d}$, leading to the $W' \times (W' - p)$

¹For example, $\mathbf{R}_{b,d} = \begin{bmatrix} 1 & 0.95 \\ 0.95 & 1 \end{bmatrix}$ and $s_1 = 1, s_2 = 3$. Then, $\mathbf{R}'_{b,d} = \begin{bmatrix} 1 & 0 & 0.95 \\ 0 & 0 & 0 \\ 0.95 & 0 & 1 \end{bmatrix}$.

noise subspace matrix \mathbf{U}'_n and thus $\mathbf{Q}' = \mathbf{U}'_n(\mathbf{U}'_n)^\dagger$. The polynomial is modified as

$$f(z) = \sum_{m=0}^{W'-1} \sum_{n=0}^{W'-1} [\mathbf{Q}']_{m,n} z^{g_{m,n}}. \quad (25)$$

where $g_{m,n} = m - n$ if packet loss is not considered, and $g_{m,n} = s''_m - s''_n$ otherwise. Here, p should be set to the maximum possible number of people, e.g., the capacity of a room. When the polynomial in (25) cannot produce results in the range $[b_{\min}, b_{\max}]$, we call $f(z) = 0$ insolvable and put an empty solution into a set $\mathcal{N}_{b,d}$. Otherwise, we save the breathing rate candidates $\{\hat{b}_1, \hat{b}_2, \dots, \hat{b}_{p'}\}$ into a set denoted as $\mathcal{S}_{b,d}$, where p' is the number of candidates after filtering as discussed in Section II-H. After processing all D links, the sets $\{\mathcal{S}_{b,d}\}_{b=1,2,\dots,D}^D$ are combined together into \mathcal{S} as $\cup_{d=1}^D \cup_{b=1}^B \mathcal{S}_{b,d}$ and \mathcal{N} as $\cup_{d=1}^D \cup_{b=1}^B \mathcal{N}_{b,d}$, where \cup denotes the set union operator.

C. Breathing Detection

Some of the breathing rate candidates generated by the breathing feature extraction might still be noisy estimations caused by interference and/or thermal noise in the CSIs. Therefore, we need to assess how likely these candidates are caused by interference and noise. If with high probability, these candidates have no correlation with human breathing, we determine that there is no people breathing. Otherwise, we conclude that breathing is present.

We observe from extensive experiments that the statistics of the set \mathcal{S} and set \mathcal{N} are indicator functions of the presence of breathing: in the absence of breathing, it is more likely that the polynomial in (25) is insolvable, which yields a large \mathcal{N} and a small \mathcal{S} in terms of their cardinalities, i.e., number of unique set elements. On the contrary, when breathing exists, solving the polynomial in (25) would produce many breathing rate candidates, giving rise to a small \mathcal{N} and a large \mathcal{S} . We leverage this observation for breathing detection.

1) *Calculating α and β* : Firstly, we formulate two statistics α and β expressed as

$$\alpha = \frac{\#(\mathcal{N})}{\#(\mathcal{S}) + \#(\mathcal{N})}, \beta = \frac{\#(\mathcal{S})}{BDp}, \quad (26)$$

where the denominator of β stands for the total number of possible breathing rate candidates with B blocks, D links, and p estimations per link per time window. $\#(\cdot)$ denotes the cardinality of a set. α indicates the *insolvability* of (25), while β indicates the *diversity* of (25). The correlation between (α, β) and the presence of breathing motivates us to develop a detection scheme based on the observed (α, β) values.

2) *Automatic Label Learning*: TR-BREATH can learn the labels y associated with each (α, β) obtained in the training phase automatically. Write $\theta = (\alpha, \beta)$ for convenience, and by convention, y equals to $+1$ if the associated θ is measured in the presence of breathing, and y equals to -1 otherwise.

During the training phase, TR-BREATH makes T observations of θ , written as $\{\theta_i\}_{i=1,2,\dots,T}$. Based on the observations, TR-BREATH extracts the labels $\{\hat{y}_i\}_{i=1,2,\dots,T}$ using unsupervised label learning consisting of two phases (i)

Partition $\{\theta_i\}_{i=1,2,\dots,T}$ into 2 classes by invoking k-means clustering [22] with $k = 2$. Denote the centroids of cluster 1 and 2 as $(\hat{\alpha}_1, \hat{\beta}_1)$ and $(\hat{\alpha}_2, \hat{\beta}_2)$, respectively. (ii) If $\hat{\alpha}_1 > \hat{\alpha}_2$, label all members of cluster 1 with $\hat{y} = -1$ to indicate that they are observed in the absence of breathing. Then, label the members of cluster 2 with $\hat{y} = +1$. Similar procedure applies to the case of $\hat{\alpha}_1 < \hat{\alpha}_2$. In the rare case that $\hat{\alpha}_1 = \hat{\alpha}_2$, label the elements within the cluster with a larger $\hat{\beta}$ with $\hat{y} = +1$.

3) *SVM Classification*: Based on $\{\theta_i\}_{i=1,2,\dots,T}$ and $\{\hat{y}_i\}_{i=1,2,\dots,T}$, we train a support vector machine (SVM) [23], a widely used binary classifier. SVM returns two weight factors ω_α and ω_β as well as a bias ω_b . ω_α and ω_β signify the importance of α and β in breathing detection. After the training phase, given any $\theta = (\alpha, \beta)$, TR-BREATH determines that breathing exists if $\omega_\alpha\alpha + \omega_\beta\beta + \omega_b > 0$ and non-existent otherwise.

D. Breathing Rate Estimation

If breathing is detected, TR-BREATH proceeds by formulating multi-person breathing rate estimation.

1) *Clustering by Affinity Propagation*: The breathing rate candidates in \mathcal{S} are fed into the affinity propagation algorithm [17]. It works by passing the responsibility message to decide which estimations are exemplars, and the availability message to determine the membership of an estimation to one of the clusters. Different from k-means [22], affinity propagation does not require the knowledge of the cluster number. Here, we assume that affinity propagation partitions the elements of \mathcal{S} into U clusters.

2) *Likelihood Assignment*: For each cluster, TR-BREATH evaluates its population, variance, and centroid, expressed as p_i , v_i , and c_i . Then, p_i and v_i are normalized as $\bar{p}_i = p_i / \sum_{i=1}^U p_i$ and $\bar{v}_i = v_i / \sum_{i=1}^U v_i$. The likelihood of cluster i , denoted by l_i , is calculated as

$$l_i = \begin{cases} 0, & (v_i = 0, p_i = 1), \text{ or } \bar{p}_i < 2\% \\ \frac{e^{\omega_p \bar{p}_i - \omega_v \bar{v}_i - \omega_c c_i}}{\sum_{i=1}^U e^{\omega_p \bar{p}_i - \omega_v \bar{v}_i - \omega_c c_i}}, & \text{Otherwise} \end{cases}, \quad (27)$$

where ω_p , ω_v , and ω_c are positive weighting factors to account for different scales of the corresponding terms. The likelihood assignment in (27) incorporates a term related to the cluster centroid c_i . The insight is that a high breathing rate is less likely than a low breathing rate in real life. Meanwhile, high breathing rate candidates are more likely to be caused by the harmonics of breathing rates. Also, (27) implies that singletons, i.e., clusters with a single element ($v_i = 0$ and $p_i = 1$), should be assigned with zero likelihoods. Clusters with $\bar{p}_i < 2\%$ are also considered as outliers and are eliminated.

3) *Cluster Merging*: Since the breathing rates are evaluated for each time window and for each link independently, it is likely that breathing rate estimations for the same person differ slightly in a small range. This results in several closely-spaced clusters, which should be merged to improve the performance.

To identify the clusters to be merged, we calculate the inter-cluster distances by calculating the differences in their centroids. Then, we merge clusters with inter-cluster distance

falling below a threshold, known as the merging radius denoted by γ . For example, if $|c_i - c_{i+1}| < \gamma$, then, cluster i and $i + 1$ would be merged. Denote the new cluster index as i' , the normalized population of cluster i' is given by $\bar{p}_{i'} = \bar{p}_i + \bar{p}_{i+1}$ and the normalized variance $\bar{v}_{i'}$ is recalculated. The centroid of cluster i' is expressed as the weighted average of the merged two clusters, given by $c_{i'} = \frac{\bar{l}_i c_i + \bar{l}_{i+1} c_{i+1}}{\bar{l}_i + \bar{l}_{i+1}}$.

Finally, the likelihood of cluster i' is updated using (27). Merging of more than two clusters can be generalized from the aforementioned steps and is omitted here for brevity. The procedures for likelihood assignment and cluster merging are highlighted in Fig. 1.

Assuming a total of \bar{K} clusters after merging and that the number of people K is known, TR-BREATH directly outputs $K_o = \min(\bar{K}, K)$ centroids with the highest likelihoods as the multi-person breathing rate estimations, i.e., $\hat{b}_i = c_{\text{idx}_i}$, $i = 1, 2, \dots, K_o$ where idx_i stands for the index of the i -th largest likelihood.

E. Estimating the Number of People

Denote the set \mathcal{J} as $\mathcal{J} = \{j | \sum_{i=1}^{\min(\bar{K}, j)} \bar{l}_{\text{idx}_i} \geq \lambda\}$ where λ is a threshold. In other words, the set \mathcal{J} contains the number of clusters with an accumulated likelihood exceeding λ . When the exact people number is unknown, given the knowledge of the maximum possible number of people, TR-BREATH formulates an estimation $\hat{K}(\lambda)$ given by the minimum element of \mathcal{J} denoted as $\hat{K}(\lambda) = \min(\mathcal{J})$, i.e., the smallest j that satisfies $\sum_{i=1}^{\min(\bar{K}, j)} \bar{l}_{\text{idx}_i} \geq \lambda$.

IV. EXPERIMENT RESULTS

A. Experiment Setups

1) *Environment*: We conduct extensive experiments to evaluate the performance of the breathing monitoring system. The experiments are conducted in three different rooms in an office suite with dimensions $5.5\text{m} \times 5\text{m}$, $8\text{m} \times 7\text{m}$, and $8\text{m} \times 5\text{m}$, respectively.

2) *Devices*: We build one pair of prototypes equipped with off-the-shelf WiFi cards with 3 omnidirectional antennas to obtain CSIs. Thus, the total number of links D is 9. One of the prototypes works as the access point (AP), while the other works as the station (STA). The center frequency is configured as 5.765 GHz with a bandwidth of 40 MHz. The transmit power is 20 dBm (100 milliwatts). The set of usable subcarriers \mathcal{V} is given as $\{-58, -57, -56, \dots, -2, 2, 3, \dots, 56, 57, 58\}$ with $V = 114$. The size of DFT is $N_{\text{DFT}} = 128$.

3) *Placement of WiFi devices*: The performance is evaluated in both LOS and NLOS scenarios. For the LOS scenarios, the AP and STA are placed in the same room with people, while for the NLOS scenarios, they are placed outside the room blocked by two walls. The locations of both WiFi devices are marked in Fig. 3.

4) *Participants*: A total of 17 different participants were invited. During the experiments, slight movements, e.g., head or limb movements, were allowed.

5) *Parameter Settings*: The following parameters are used unless otherwise stated:

- Each experiment lasts for 2 minutes.
- The signal subspace dimension p is configured as 10.
- The merging radius γ is set as 0.5 BPM.
- The range of interest of the breathing rate is from $b_{\min} = 10$ BPM to $b_{\max} = 50$ BPM. This covers the adult breathing rate at rest (10–14 BPM), infant breathing rate (37 BPM), and the breathing rate after workout [24], [25].
- The packet rate of WiFi transmission is 10 Hz^2 .
- The sampling interval T_{sp} is 0.1s where s stands for second. For notational convenience, we write the time duration of each block measured in seconds as $M_t = MT_{sp}$ and the window size measured in seconds as $W_t = WT_{sp}$. The overlap in terms of seconds between different blocks is $P_t = PT_{sp}$. As default values, we adopt the parameters $M_t = 45\text{s}$, $W_t = 40.5\text{s}$, $P_t = 4.5\text{s}$, and $B = 5$ unless otherwise stated. The total time of CSI measurements T_{tot} is thus $M_t + (B - 1) \times P_t$ which equals to 63s.

During the experiments, we only observe 2 ~ 3 WiFi networks sharing the same WiFi channel with the experimental devices, leading to less than 1% packet loss rate for all experiments. The impact of packet loss can be safely ignored in this case. Therefore, (25) reduces to (21), and we use $g_{m,n} = m - n$ in (22). Meanwhile, M equals to M' as shown in Fig. 2.

6) *Ground-Truths*: The performance of the proposed monitoring system is evaluated by comparing the breathing rate estimations against the ground-truths. To obtain the ground-truths, we ask each participant to synchronize his/her breathing according to a metronome application on his/her cellphone. After the controlled breathing experiments, we conduct experiments in a more practical setting where the participants are asked to breathe naturally according to their personal habits and count their own breathing rates manually.

B. Metrics for Performance Evaluation

1) *Breathing Detection Rate*: The detection performance of the proposed system is directly determined by the SVM classification accuracy, which is evaluated by performing K -fold cross-validation on the SVM classifier.

2) *Breathing Rate Estimation Accuracy*: Assume that K is known in advance with ground-truths given by $\mathbf{b} = [b_1, b_2, \dots, b_K]$, and the proposed system outputs $K_o = \min(\bar{K}, K)$ estimations denoted as $\hat{\mathbf{b}} = [\hat{b}_1, \hat{b}_2, \dots, \hat{b}_{K_o}]$, the accuracy of estimation is calculated as $\left(1 - \frac{1}{K_o} \sum_{i=1}^{K_o} \left| \frac{\hat{b}_i - b_i}{b_i} \right| \right) \times 100\%$. For instance, the accuracy calculated from $\hat{\mathbf{b}} = [25.1, 29.8]$ BPM and $\mathbf{b} = [25, 30]$ BPM is 99.5%.

²The 10Hz packet rate agrees with the *beaconing rate* of a commercial WiFi AP, and the packet size containing one CSI measurement is 2.5KB, resulting in a data rate of 25KB/s during CSI acquisition. Therefore, the proposed system only introduces minor interference to the co-existing WiFi networks on the same WiFi channel.

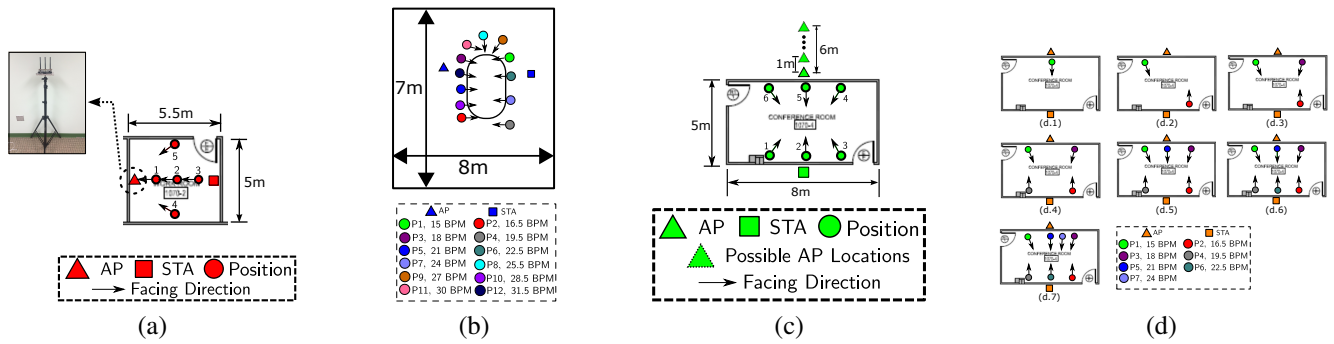


Fig. 3: Experiment settings: (a) single-person, LOS (b) multi-person, LOS (c) single-person, NLOS (d) multi-person, NLOS.

3) *Average K_o* : Still assuming that K is known and the monitoring system outputs $K_o = \min(\bar{K}, K)$ estimations. In this case, there is no penalty if $\bar{K} \geq K$ since the breathing rates estimations are given by the first K estimations with the highest likelihoods. On the other hand, when $\bar{K} < K$, the breathing rates associated with $K - \bar{K}$ people are missing in the estimations. Therefore, the average of K_o , denoted as \bar{K}_o , is also an important metric, as \bar{K}_o closer to K indicates that most of the human breathing rates can be resolved by the monitoring system.

4) *Estimation Error of Number of People*: When K is unknown, we formulate an estimation on the number of people K via $\hat{K}(\lambda)$, with the performance evaluated by the function $P(\lambda) = E(|K - \hat{K}(\lambda)|)$, where E stands for the expectation operator.

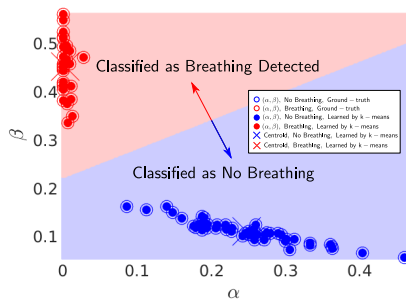


Fig. 4: Classification performance for breathing detection.

C. Breathing Detection Performance

The proposed breathing detection scheme determines the existence of breathing based on the output of the SVM algorithm. We use 84 CSI measurements for evaluation, where 32 of them are collected in the presence of at least one person breathing, and 52 measurements are obtained without people breathing in the room. The devices are placed according to the NLOS setting shown in Fig. 3(c).

In Fig. 4, we demonstrate the breathing detection performance of the proposed system. First of all, we observe that the labels \hat{y} can be inferred from (α, β) without errors. Secondly, we observe that SVM returns a hyperplane that partitions (α, β) perfectly, implying a 100% detection rate. This is further validated by performing K-fold cross-validation on the results, leading to a 100% accuracy for each cross-validation.

D. Performance of Breathing Rate Estimation

In this part, we evaluate the performance of the proposed system based on the ground-truth breathing rates using metronomes.

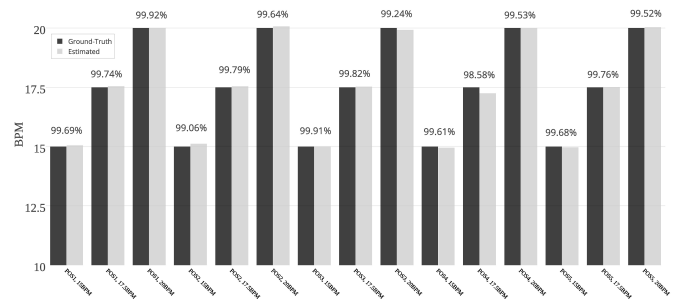


Fig. 5: Accuracy with single-person breathing under the LOS scenario. $M_t = 45s$, $W_t = 40.5s$, $P_t = 4.5s$, $B = 5$, and $T_{tot} = 63s$.

1) *Accuracy under Single-Person LOS Scenario*: We ask one participant to sit at 5 positions as shown in Fig. 3(a) under the LOS scenario. For each position, the participant breathes at 15 BPM in synchronization to the metronome. After that, the participant switches the breathing rate to 17.5 BPM and later 20 BPM. The accuracy performances at the 5 positions with various breathing rates are depicted in Fig. 5. For comparison purpose, Fig. 5 also demonstrates the ground-truths. As can be seen from the figure, the proposed system can estimate the breathing rate with an accuracy of 99.56% averaging over all cases. The worst case is when the participant sits at position 4 and breathes at 17.5 BPM with an accuracy of 98.58%, equivalent to an estimation error of ± 0.249 BPM.

2) *Accuracy under Multi-Person LOS Scenario*: A total of 12 people were invited into the conference room as shown in Fig. 3(b) under the LOS scenario. The details of the position and breathing rate for each participant are displayed in Fig. 3(b). The normalized population, variance, likelihood, and centroid for each cluster are presented in Fig. 6. It can be seen that the proposed system resolves the breathing rates of 9 out of a dozen people with an accuracy of 98.65%.

3) *Accuracy under Single-Person NLOS Scenario*: One participant was invited into the conference room to breathe with 15 BPM at 6 different positions, with details shown in

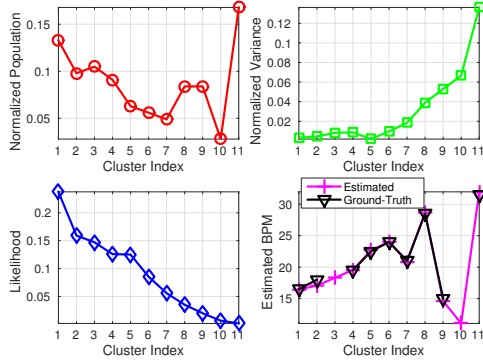


Fig. 6: Performance of estimating breathing rates of a dozen people under the LOS scenario. $M_t = 45s$, $W_t = 40.5s$, $P_t = 4.5s$, $B = 5$, and $T_{tot} = 63s$.

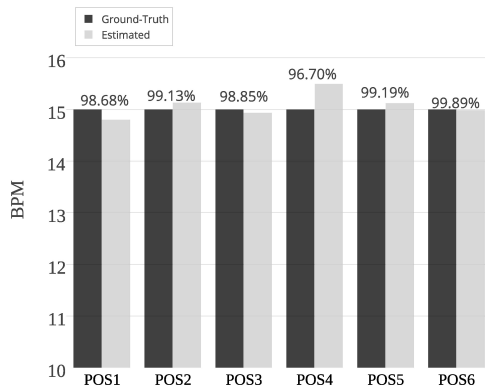


Fig. 7: Accuracy with single-person breathing under the NLOS scenario. $M_t = 45s$, $W_t = 40.5s$, $P_t = 4.5s$, $B = 5$, and $T_{tot} = 63s$.

Fig. 3(c). Both WiFi devices are placed outside the conference room. Fig. 7 shows that a mean accuracy of 98.74% averaging over the 6 positions is achieved even when the two devices are blocked by two concrete walls of the conference room, which validates the high accuracy under the through-the-wall scenario.

To evaluate the impact of distances between WiFi devices on the performance, we place the AP at 6 different locations with 1 meter resolution. The participant breathes at 15 BPM

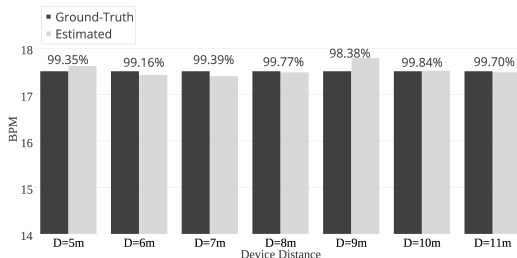


Fig. 8: Accuracy of breathing rate estimation with various distances. $M_t = 45s$, $W_t = 40.5s$, $P_t = 4.5s$, $B = 5$, and $T_{tot} = 63s$.

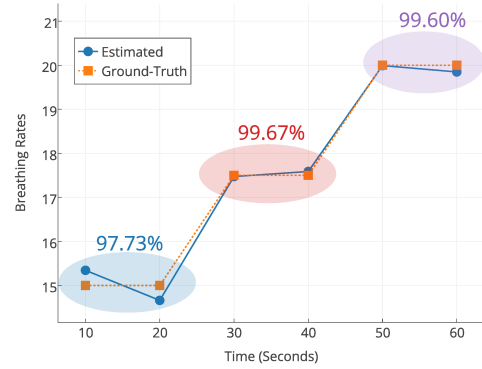


Fig. 9: Accuracy of breathing rate estimation with 10 seconds of CSI measurement. $M_t = 10s$, $W_t = 9s$, $P_t = 0.5s$, $B = 1$, and $T_{tot} = 10s$.

in this experiment. The distance between the AP and the STA ranges from 5 meters to 11 meters. As shown in Fig. 8, the proposed scheme achieves more than 98.38% in accuracy, with a mean accuracy of 99.37% averaging over the results of various distances. Even when the device distance reaches 11 meters, the accuracy is maintained at 99.70%, demonstrating the robustness of the proposed system under different device distances.

We further evaluate TR-BREATH by reducing M_t to 10s. Besides, we set $W_t = 9s$, $P_t = 0.5s$, and $T_{tot} = 10s$. The packet rate is increased to 30 Hz. One participant sits at position 1 of Fig. 3(c) and breathe at 15, 17.5, 20 BPM, with each breathing rate lasting for 20 seconds. The total measurement time is 60 seconds. Fig. 9 shows that TR-BREATH could track the breathing rate accurately with a mean accuracy of 99%. Therefore, TR-BREATH can provide accurate breathing rates every 10 second for single-person breathing monitoring that fits well to the patient monitoring scenarios.

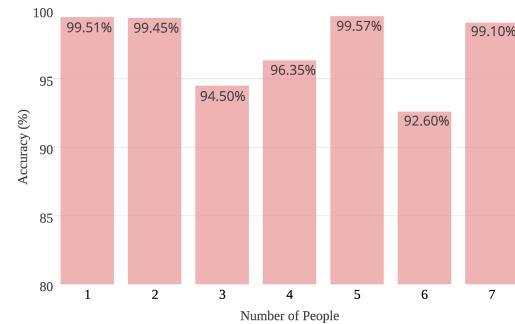


Fig. 10: Accuracy with multiple people under the NLOS scenario. $M_t = 45s$, $W_t = 40.5s$, $P_t = 4.5s$, $B = 5$, and $T_{tot} = 63s$.

4) *Accuracy under Multi-Person NLOS Scenario:* We invite up to 7 people into one conference room with two devices placed under the NLOS scenario. The positions and breathing rates associated with each person are depicted in Fig. 3(d). Fig. 10 summarizes the accuracy performances, which shows

that an accuracy of 99.1% when $K = 7$ and a mean accuracy of 97.3% averaging over all 7 cases can be achieved.

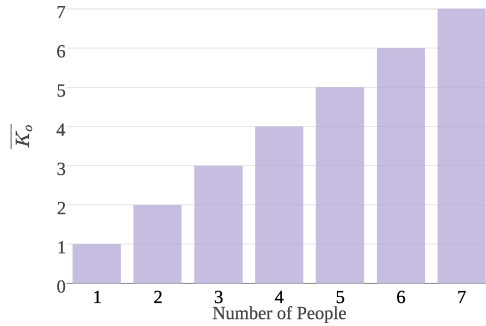


Fig. 11: \overline{K}_o with multiple people under the NLOS scenario. $M_t = 45s$, $W_t = 40.5s$, $P_t = 4.5s$, $B = 5$, and $T_{tot} = 63s$.

5) \overline{K}_o under Multi-Person NLOS Scenario: Fig. 11 demonstrates the \overline{K}_o performance for the multi-person NLOS scenario. As we can see, with a various number of people K , \overline{K}_o equals to K , which shows that the proposed system could resolve the breathing rates of all people. Combining the results in Fig. 10, we conclude that given K people, the proposed system resolves the breathing rates of K people with high accuracy.

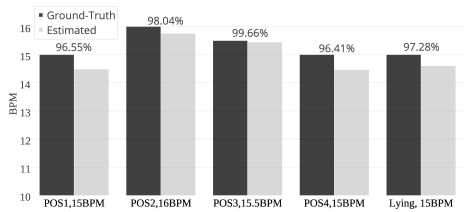


Fig. 12: Performance of estimating the natural breathing rates of one person under the NLOS scenario. $M_t = 45s$, $W_t = 40.5s$, $P_t = 4.5s$, $T_{tot} = 63s$.

E. Performance of Natural Breathing Rate Estimation

In this part, we investigate the performance of the proposed system in a more practical setting by asking the participants to breathe naturally. Instead of using the metronomes, the participants were asked to memorize how many breaths they took in a minute.

1) Accuracy under Single-Person NLOS Scenario: One participant is asked to breathe naturally at 4 different positions in the same conference room as in Fig. 3(c). Then, the participant lies on the ground and breathe. Fig. 12 shows that a mean accuracy of 97.0% can be achieved. Moreover, the breathing rate of a person lying on the ground can be estimated accurately, which shows the viability of the proposed scheme in monitoring the breathing rate of a sleeping person.

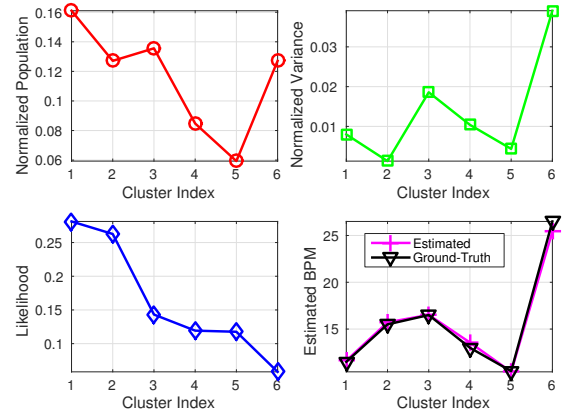


Fig. 13: Performance of estimating the natural breathing rates of 9 people under the NLOS scenario. $M_t = 45s$, $W_t = 40.5s$, $P_t = 4.5s$, $T_{tot} = 63s$.

2) Accuracy under Multi-Person NLOS Scenario: Nine participants breathe naturally in the conference room shown in Fig. 3(c). The breathing rates are given as [16, 11.5, 10.5, 12, 13, 15.5, 16.5, 26.5, 12] BPM, where two participants coincide in their breathing rates. Fig. 13 shows that 6 out of the 8 resolvable breathing rates are obtained with an accuracy of 98.07%.

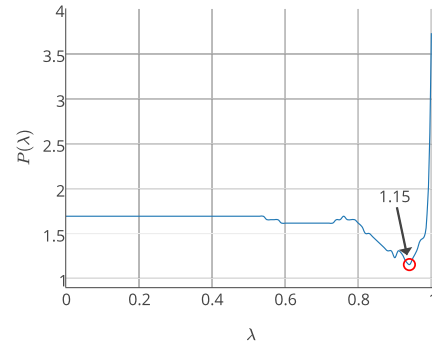


Fig. 14: Performance of people number estimation. $M_t = 45s$, $W_t = 40.5s$, $P_t = 4.5s$, $B = 5$, and $T_{tot} = 63s$.

F. Estimating the Number of People K

Fig. 14 illustrates that the optimal $P(\lambda)$ is 1.15 when $\lambda = 0.88$. Thus, the proposed system can estimate the number of people with an error around 1.

V. IMPACT OF VARIOUS FACTORS

In this section, we further investigate the performance of TR-BREATH in a more practical application scenario. First of all, we study the performance under the influence of packet loss with various severity. Then, we discuss the effects of motions on TR-BREATH. Finally, we demonstrate the significant improvement of TR-BREATH using both amplitude and phase information compared to the approach using amplitude only in [5]. The parameters are configured to be the same as Section IV-A5 unless otherwise stated.

A. Impact of Packet Loss

We present the accuracy under the NLOS single-person at position 1 shown in Fig. 3(c) with different packet loss rate. We consider two packet loss mechanism, i.e., bursty packet loss and random packet loss. The bursty packet loss is mainly caused by the continuous data transmission among few WiFi devices which fully jams the medium for a long time. On the other hand, the random packet loss is due to the random access of a large number of nearby WiFi devices which occupy the medium occasionally.

To emulate packet loss, we intentionally discard collected CSI samples in the experiments. More specifically, for the bursty packet loss, we discard CSI samples within a certain time period, while for the random packet loss, we discard CSI samples with index following a uniform distribution. When the packet loss compensation is enabled, $g_{m,n} = s''_m - s''_n$ is used, otherwise $g_{m,n} = m - n$.

The results with different packet loss rate with the aforementioned two mechanisms are shown in Fig. 15. We observe that the consequence of random packet loss is much more severe than the bursty packet loss when the packet loss compensation is not enabled. With 10% random packet loss, the accuracy drops to 88.35% from 99.35%. The accuracy further deteriorates to 74.13% and 62.83% with 20% and 30% packet loss, respectively. The advantage of packet loss compensation is obvious since TR-BREATH maintains an accuracy of 99.70% even with 30% packet loss. On the contrary, bursty packet loss does not degrade the accuracy greatly. It can be justified by the fact that most CSIs are still sampled uniformly under this scenario.

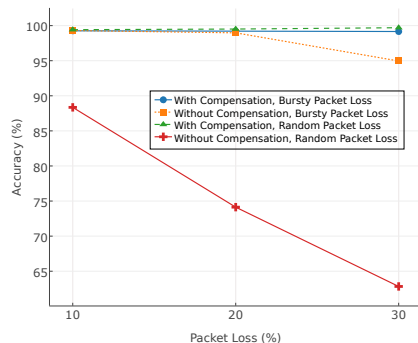


Fig. 15: Impact of packet loss on accuracy

B. Impact of Motion

To study the effect of motion, we perform additional experiments involving ambient motions and subject motions. The experiment settings are shown in Fig. 16. The participant breathes at 20 BPM.

1) *Impact of Ambient Motion:* Besides the participant under breathing monitoring, we ask another participant to walk randomly in the eight highlighted areas in Fig. 16, where S_1 to S_4 stands for the ambient motions in the conference room and S_5 to S_8 in the foyer. We further classify these areas in terms of their distances to the WiFi AP as very close, close,

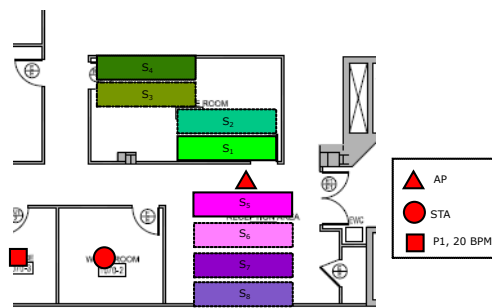


Fig. 16: Experiment settings for investigation of ambient motions and subject motions

far, and very far. For instance, S_1 is considered to be very close from the WiFi AP, while S_4 is regarded as very far away from the WiFi AP. Despite that the impact of motion is location-dependent, in general, we find that the motions introduce severe interference into TR-BREATH when they occur within 1m radius to either the AP or the STA.

The results are depicted in Fig. 17. Clearly, when the ambient motion occurs very close to the WiFi AP, the accuracy degrades significantly, especially for the case of ambient motions in the foyer area indicated by S_5 . When the distance between the motion to the WiFi AP increases, the accuracy is improved. We observe similar results when the ambient motion occurs close to the WiFi device. Thus, we conclude that TR-BREATH can tolerate ambient motions as long as both WiFi devices of TR-BREATH are far from these motions.

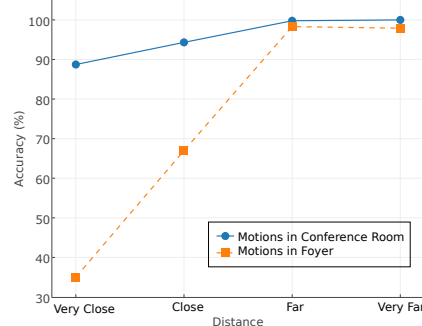


Fig. 17: Impact of ambient motion on accuracy

2) *Impact of Subject Motion:* In this experiment, we ask the participant under monitoring to move randomly for a certain period of time, and then sit back to the original position as shown in Fig. 16 to continue breathing. The results are shown in Fig. 18. We observe that when the participant only moves for 10 seconds, the accuracy can be maintained at 95.96%. The accuracy drops to 87.61% when the participant moves for 40 seconds, corresponding to an error of ± 2.48 BPM. This demonstrates that TR-BREATH can tolerate the subject motions given that the participant stays still during most of the time.

3) *Impact of using CSI Amplitude Only:* Thanks to the additional step of CSI calibration mentioned in Section III, TR-BREATH makes full use of the complex CSIs, which is

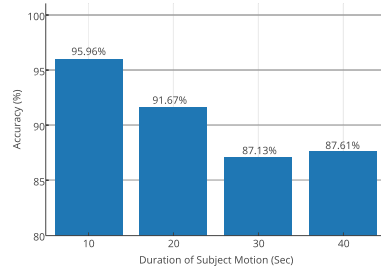


Fig. 18: Impact of subject motion on accuracy

a major difference from [5] which uses the CSI amplitudes only. In this section, we show that using both CSI amplitudes and phases could improve the performance of TR-BREATH. Furthermore, we replace the Root-MUSIC algorithm with the conventional Welch estimator [26], a widely used non-parametric scheme. For the Welch estimator, we use the CSI amplitude only, which coincides with the spectral analysis scheme used in [5].

We ask the participant to breathe at [20, 25, 30, 35, 40, 45] BPM under the setting of Fig. 16 without ambient and subject motions. Each experiment lasts for 1 minute. The cumulative density functions (CDFs) of the accuracy for this experiment are shown in Fig. 19. We observe that the results are more concentrated in areas close to 100% accuracy in the complex CSI case, indicating that using complex CSIs outperforms the amplitude-only case and the Welch estimator.

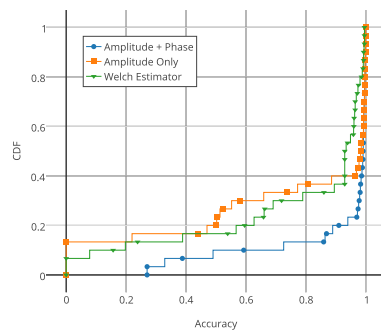


Fig. 19: Comparison of CDFs among different schemes

VI. FUTURE WORK

As a future work, we would conduct long-term experiments to investigate the performance of TR-BREATH in the long run. Meanwhile, we would investigate the way to detect and discard CSI samples significantly affected by subject and ambient motions so as to further enhance the robustness of TR-BREATH.

VII. CONCLUSION

In this paper, we present TR-BREATH, a contact-free and highly accurate breathing monitoring system leveraging TR for breathing detection and multi-person breathing rate

estimations using commercial WiFi devices. The TR resonating strengths are analyzed by the Root-MUSIC algorithm to extract features for breathing detection and breathing rate estimation. Experiment results in a typical indoor environment demonstrate that, with 63 seconds of measurements, a perfect detection rate can be obtained. Meanwhile, the proposed system can estimate the single-person breathing rate in the NLOS scenario with an accuracy of 99% with only 10 seconds of measurement. With 63 seconds of measurement, the proposed system achieves a mean accuracy of 98.65% for a dozen people under the LOS scenario and 98.07% for 9 people under the NLOS scenario even when the two WiFi devices are blocked by two walls. The proposed system can also estimate the number of people with an average error around 1. We also show that TR-BREATH is robust against packet loss and motions in the environment. With the ubiquity of WiFi-enabled mobile devices, TR-BREATH can provide real-time, in-home, and non-invasive breathing monitoring in the future medical applications.

REFERENCES

- [1] "Vital signs." <http://www.hopkinsmedicine.org/>.
- [2] B.-K. Park, S. Yamada, O. Boric-Lubecke, and V. Lubecke, "Single-channel receiver limitations in doppler radar measurements of periodic motion," in *Radio and Wireless Symposium, 2006 IEEE*, pp. 99–102, Jan 2006.
- [3] F. Adib, H. Mao, Z. Kabelac, D. Katabi, and R. C. Miller, "Smart homes that monitor breathing and heart rate," in *Proceedings of the 33rd Annual ACM Conference on Human Factors in Computing Systems, CHI '15*, (New York, NY, USA), pp. 837–846, ACM, 2015.
- [4] H. Abdelnasser, K. A. Harras, and M. Youssef, "UbiBreath: A ubiquitous non-invasive WiFi-based breathing estimator," in *Proceedings of the 16th ACM International Symposium on Mobile Ad Hoc Networking and Computing, MobiHoc '15*, (New York, NY, USA), pp. 277–286, ACM, 2015.
- [5] J. Liu, Y. Wang, Y. Chen, J. Yang, X. Chen, and J. Cheng, "Tracking vital signs during sleep leveraging off-the-shelf WiFi," in *Proceedings of the 16th ACM International Symposium on Mobile Ad Hoc Networking and Computing, MobiHoc '15*, pp. 267–276, 2015.
- [6] C. Chen, Y. Han, Y. Chen, and K. J. R. Liu, "Multi-person breathing rate estimation using time-reversal on WiFi platforms," in *2016 IEEE Global Conference on Signal and Information Processing (GlobalSIP)*, December 2016. To appear.
- [7] B. D. Rao and K. V. S. Hari, "Performance analysis of root-music," *IEEE Trans. Acoust., Speech, Signal Processing*, vol. 37, pp. 1939–1949, Dec 1989.
- [8] Y. Chen, F. Han, Y. H. Yang, H. Ma, Y. Han, C. Jiang, H. Q. Lai, D. Claffey, Z. Safar, and K. J. R. Liu, "Time-reversal wireless paradigm for green internet of things: An overview," *IEEE Internet Things J.*, vol. 1, pp. 81–98, Feb 2014.
- [9] C. Chen, Y. Chen, Y. Han, H. Q. Lai, and K. J. R. Liu, "Achieving centimeter-accuracy indoor localization on WiFi platforms: A frequency hopping approach," *IEEE Internet Things J.*, vol. 4, pp. 111–121, Feb 2017.
- [10] C. Chen, Y. Chen, Y. Han, H. Q. Lai, F. Zhang, and K. J. R. Liu, "Achieving centimeter-accuracy indoor localization on WiFi platforms: A multi-antenna approach," *IEEE Internet Things J.*, vol. 4, pp. 122–134, Feb 2017.
- [11] C. Chen, Y. Han, Y. Chen, and K. J. R. Liu, "Indoor global positioning system with centimeter accuracy using Wi-Fi [applications corner]," *IEEE Signal Processing Mag.*, vol. 33, pp. 128–134, Nov 2016.
- [12] Z.-H. Wu, Y. Han, Y. Chen, and K. J. R. Liu, "A time-reversal paradigm for indoor positioning system," *IEEE Trans. Veh. Commun.*, vol. 64, pp. 1331–1339, April 2015.
- [13] F. Zhang, C. Chen, B. Wang, H.-Q. Lai, and K. J. R. Liu, "A time-reversal spatial hardening effect for indoor speed estimation," in *2017 IEEE International Conference on Acoustics, Speech, and Signal Processing (ICASSP)*, March 2017. To appear.

- [14] Q. Xu, Y. Chen, B. Wang, and K. J. R. Liu, "Radio biometrics: Human recognition through a wall," *IEEE Trans. Inf. Forensics Security*, vol. 12, pp. 1141–1155, May 2017.
- [15] Q. Xu, Y. Chen, B. Wang, and K. J. R. Liu, "TRIEDS: Wireless events detection through the wall," *IEEE Internet Things J.*, vol. PP, no. 99, pp. 1–1, 2017.
- [16] B. Wang, Y. Wu, F. Han, Y.-H. Yang, and K. J. R. Liu, "Green wireless communications: A time-reversal paradigm," *IEEE J. Select. Areas Commun.*, vol. 29, pp. 1698–1710, September 2011.
- [17] B. J. Frey and D. Dueck, "Clustering by passing messages between data points," *Science*, vol. 315, p. 2007, 2007.
- [18] N. V. Rivera, S. Venkatesh, C. Anderson, and R. M. Buehrer, "Multi-target estimation of heart and respiration rates using ultra wideband sensors," in *Signal Processing Conference, 2006 14th European*, pp. 1–6, Sept 2006.
- [19] A. Goldsmith, *Wireless Communications*. New York, NY, USA: Cambridge University Press, 2005.
- [20] M. Abramowitz, *Handbook of Mathematical Functions, With Formulas, Graphs, and Mathematical Tables.*. Dover Publications, Incorporated, 1974.
- [21] R. Schmidt, "Multiple emitter location and signal parameter estimation," *IEEE Trans. Antennas Propagat.*, vol. 34, pp. 276–280, Mar 1986.
- [22] J. MacQueen, "Some methods for classification and analysis of multivariate observations," in *Proceedings of the Fifth Berkeley Symposium on Mathematical Statistics and Probability, Volume 1: Statistics*, (Berkeley, Calif.), pp. 281–297, University of California Press, 1967.
- [23] C. J. C. Burges, "A tutorial on support vector machines for pattern recognition," *Data Min. Knowl. Discov.*, vol. 2, pp. 121–167, June 1998.
- [24] J. F. Murray, *The normal lung : the basis for diagnosis and treatment of pulmonary disease / John F. Murray*. Saunders Philadelphia, 1976.
- [25] M. Kearon, E. Summers, N. Jones, E. Campbell, and K. Killian, "Breathing during prolonged exercise in humans," *The Journal of physiology*, vol. 442, p. 477, 1991.
- [26] P. Welch, "The use of fast Fourier transform for the estimation of power spectra: A method based on time averaging over short, modified periodograms," *IEEE Trans. Audio Electroacoust.*, vol. 15, pp. 70–73, Jun 1967.



Chen Chen (S'15) received the B.S. and M.S. degrees from the Department of Microelectronics, Fudan University, Shanghai, China, in 2010 and 2013, respectively. He is currently pursuing the Ph.D. degree at the Department of Electrical and Computer Engineering, University of Maryland at College Park, College Park, MD, USA.

His research interests include biomedical signal processing, indoor localization, and wireless communications.

Mr. Chen was the recipient of multiple honors and awards, including the Best Student Paper Award of the IEEE ICASSP 2016, the Litton Industries Fellowship from the University of Maryland at College Park in 2015, the Distinguished Graduate Student Teaching Award from the University of Maryland at College Park in 2014, and the Excellent Graduate Student of Shanghai in 2013.



Yi Han (GS'14 – M'15) received the B.S. degree in electrical engineering (with highest honor) from Zhejiang University, Hangzhou, China, in 2011, and the Ph.D. degree from the Department of Electrical and Computer Engineering, University of Maryland at College Park, College Park, MD, USA.

He is currently the Wireless Architect with Origin Wireless Inc., Greenbelt, MD, USA. His research interests include wireless communication and signal processing.

Dr. Han was the recipient of Best Student Paper Award of IEEE ICASSP in 2016 and the Class A Scholarship from Chu Kochen Honors College, Zhejiang University in 2008.



Yan Chen (SM'14) received the bachelors degree from the University of Science and Technology of China, Hefei, China, in 2004, the M.Phil. degree from the Hong Kong University of Science and Technology, Hong Kong, in 2007, and the Ph.D. degree from the University of Maryland at College Park, College Park, MD, USA, in 2011.

Being a founding member, he joined Origin Wireless Inc., Greenbelt, MD, USA, as a Principal Technologist in 2013. He is currently a Professor with the University of Electronic Science and Technology of China, Chengdu, China. His research interests include multimedia, signal processing, game theory, and wireless communications.

Dr. Chen was the recipient of multiple honors and awards, including the Best Student Paper Award of IEEE ICASSP in 2016, the Best Paper Award of IEEE GLOBECOM in 2013, the Future Faculty Fellowship and Distinguished Dissertation Fellowship Honorable Mention from the Department of Electrical and Computer Engineering in 2010 and 2011, the Finalist of the Deans Doctoral Research Award from the A. James Clark School of Engineering, University of Maryland at College Park in 2011, and the Chinese Government Award for outstanding students abroad in 2010.



Hung-Quoc Lai (M'11) received the B.S. (*cum laude*), M.S., and Ph.D. degrees in electrical engineering from the University of Maryland at College Park, College Park, MD, USA, in 2004, 2006, and 2011, respectively.

He is a founding member and currently the Vice President of Engineering with Origin Wireless Inc., Greenbelt, MD, USA, which develops advanced time reversal wireless technologies for use in a wide variety of applications of indoor positioning/tracking, monitoring, security, radio human biometrics, wireless power transfer, and 5G communications.

Prior to joining Origin Wireless Inc. in 2013, he was a Technical Lead in research and development of multiple-input multiple-output (MIMO) and cooperative communications with the U.S. Army RDECOM CERDEC, Aberdeen Proving Ground, MD, USA. He is a Gates Millennium Scholar.



Feng Zhang (S'11) received the B.S. and M.S. degrees from the Department of Electronic Engineering and Information Science, University of Science and Technology of China, Hefei, China, in 2011 and 2014, respectively. He is currently pursuing the Ph.D. degree at the Department of Electrical and Computer Engineering, University of Maryland at College Park, College Park, MD, USA.

His research interests include time reversal communications, wireless signal processing, and indoor localization.

Mr. Zhang was a recipient of the Distinguished Graduate Student Teaching Award of the University of Maryland at College Park in 2015 and the China National Scholarship in 2014.



Beibei Wang (SM'15) received the B.S. degree in electrical engineering (with the highest honor) from the University of Science and Technology of China, Hefei, in 2004, and the Ph.D. degree in electrical engineering from the University of Maryland, College Park in 2009. She was with the University of Maryland as a research associate in 2009-2010, and with Qualcomm Research and Development in 2010-2014. Since 2015, she has been with Origin Wireless Inc. as a principal technologist.

Her research interests include wireless communications and signal processing.

Dr. Wang received the Graduate School Fellowship, the Future Faculty Fellowship, and the Deans Doctoral Research Award from the University of Maryland, and the Overview Paper Award from IEEE Signal Processing Society in 2015. She is a co-author of *Cognitive Radio Networking and Security: A Game-Theoretic View* (Cambridge University Press, 2010).



K. J. Ray Liu (F'03) was named a Distinguished Scholar-Teacher of University of Maryland, College Park, in 2007, where he is Christine Kim Eminent Professor of Information Technology. He leads the Maryland Signals and Information Group conducting research encompassing broad areas of information and communications technology with recent focus on smart radios for smart life.

Dr. Liu was a recipient of the 2016 IEEE Leon K. Kirchmayer Technical Field Award on graduate teaching and mentoring, IEEE Signal Processing Society 2014 Society Award, and IEEE Signal Processing Society 2009 Technical Achievement Award. Recognized by Thomson Reuters as a Highly Cited Researcher, he is a Fellow of IEEE and AAAS.

Dr. Liu is a member of IEEE Board of Director. He was President of IEEE Signal Processing Society, where he has served as Vice President Publications and Board of Governor. He has also served as the Editor-in-Chief of IEEE Signal Processing Magazine.

He also received teaching and research recognitions from University of Maryland including university-level Invention of the Year Award; and college-level Poole and Kent Senior Faculty Teaching Award, Outstanding Faculty Research Award, and Outstanding Faculty Service Award, all from A. James Clark School of Engineering.